CrystEngComm

COMMUNICATION

View Article Online
View Journal | View Issue

Check for updates

Cite this: *CrystEngComm*, 2025, **27**, 5095

Received 20th May 2025,
Accepted 9th July 2025

DOI: 10.1039/d5ce00520e

rsc.li/crystengcomm

Published on 10 2025. Downloaded on 29/11/2025 00:12:04.

3D ED for the localization of cations in potassium exchanged and partially dehydrated nano Y zeolite†

Yacine Malik Chaib Draa,[ab] Taylan Örs,[ab] Irena Deroche,[ab] Catherine Dejoie[c] and Jean-Louis Paillaud *[ab]

Zeolites, microporous crystalline aluminosilicates, play a vital role in catalysis and adsorption. Cation positioning strongly affects their properties but is difficult to determine in nano-zeolites due to limitations of conventional diffraction techniques. In this study, precession electron diffraction tomography (PEDT) was used to localize K^+ cations in synthetic nano-faujasite. Applying dynamical theory enabled accurate nanoscale characterization despite small crystal size. The experimental results were successfully compared with distributions from Monte Carlo simulations.

Cations in zeolites compensate for the negative charges arising from aluminium substitution for silicon in the crystal lattice. Optimizing zeolite functionality strongly depends on their distribution. However, locating cations—especially in nano-zeolites—is challenging due to the limitations of conventional X-ray diffraction (XRD) and small crystal sizes. The latter precludes single-crystal XRD, while overlapping peaks in powder XRD reduce accuracy. Cation distribution within pores is influenced by factors such as temperature, cation concentration per unit cell (u.c.), cation type, and the presence of adsorbed molecules. To describe this distribution, we refer to Smith's[1] classification of cation sites as shown in Fig. 1.

This research aims to address these challenges using three-dimensional electron diffraction (3D ED),[2–4] which enables structural characterization of zeolites at the nanoscale. These techniques reduce dynamical effects and allow high-quality data collection from small crystals. While previous studies have investigated K^+ cation locations in Y zeolites with **FAU** topology,[5–7] none have examined cation distribution in nano-zeolites of this type.

Conventional X-ray diffraction techniques are unsuitable for investigating nanometric crystals, highlighting the importance of using 3D ED for materials of this type. In this study, we used 3D ED with precession on a transmission electron microscope (TEM) to examine the distribution of K^+ in a nano-Y zeolite. Initially, nano-Y zeolite was synthesized according to the protocol established by Borel *et al.*[8] and reported in the section 1.1 of the experimental procedure in the ESI.† After synthesis, the product was characterized by powder X-ray diffraction (PXRD) and scanning electron microscopy (SEM), confirming that the sample is a nano faujasite Y with an average crystal size of about 300 ± 200 nm (sections 1.2 and 1.3 and Fig. S1 and S2 in the ESI†).

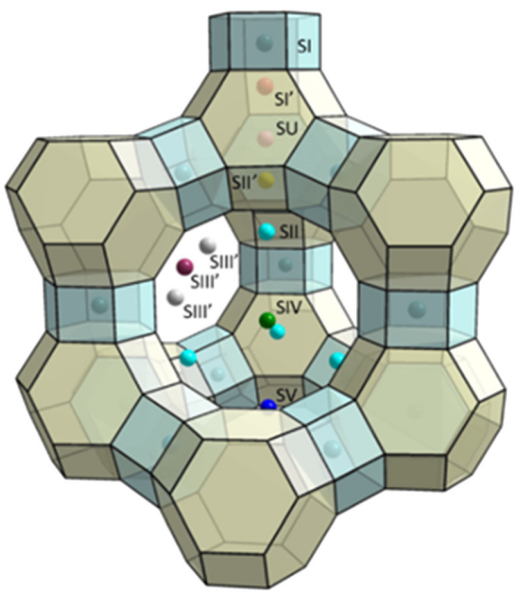

Fig. 1 Specific cation sites (SI, SI′, SU, SII, SIII, SIII′, SIV and SV) in the faujasite zeolite structure following the nomenclature proposed by Smith.[1] The hexagonal prisms and truncated octahedra (sodalite cages) are represented as blue and yellow polyhedra, respectively.

[a] *Université de Haute-Alsace, Institut de Science des Matériaux de Mulhouse (IS2M), UMR CNRS 7361, 15 Rue Jean Starcky, 68100 Mulhouse, France. E-mail: jean-louis.paillaud@uha.fr*

[b] *Université de Strasbourg, 67000 Strasbourg, France*

[c] *European Synchrotron Radiation Facility, 71 avenue des Martyrs, 38000 Grenoble, France*

† Electronic supplementary information (ESI) available: Includes the experimental procedure of synthesis and characterisation, the structural data for K-Y after kinematical, dynamical and Rietveld refinements. CCDC 2452355 and 2470815. See DOI: https://doi.org/10.1039/d5ce00520e

Published on 10 2025. Downloaded on 29/11/2025 00:12:04.

In a second step, the nano faujasite Y in its sodium form was exchanged with KCl in order to produce the potassium form K-Y. Energy dispersive X-ray spectroscopy (EDX) analysis determined the molar composition of the exchanged Y zeolite, K-Y: $K_{57.6}[Si_{134,4}Al_{57,6}O_{384}]$ (Fig. S3 in the ESI†). The Le Bail fit performed on the PXRD pattern of the hydrated exchanged Y zeolite confirms the sample's purity (Fig. S4 in the ESI†). Thermogravimetric analysis of the fully hydrated sample conducted in air reveals a total weight loss of ≈18%, corresponding to the presence of about 167 adsorbed water molecules per unit cell (section 1.4 and Fig. S5 in the ESI†). Of these, 95% are desorbed in a single step between room temperature and 210 °C, while the remaining 5% (≈8.3 molecules per u.c.) are released in a second step occurring between 210 and 380 °C.

Then, 3D electron diffraction (ED) measurements were performed in precession electron diffraction tomography (PEDT) mode on a crystal measuring about ~200 × 285 nm (section 1.5 and Fig. S2 in the ESI†). The data were then processed using the PETS2.0 software,[9] which provides an initial assessment of data quality and prepares them for further structural analysis (section 2.1 in the ESI†). Reconstructed reciprocal-space sections *hhl*, 0*kl* and *hk*1 are shown in Fig. 2. Kinematical and dynamical refinements were next performed using the JANA2020 software (section 2.2 in the ESI†).[10]

The structural solution obtained using the charge-flipping algorithm implemented in JANA2020, applied to the extracted intensities, directly revealed the positions of the Si, Al, and O framework atoms of the zeolite. However, additional steps were necessary, including an iterative process of difference Fourier map calculations, to accurately determine the positions of the extra-framework species (K^+ cations and adsorbed water molecules). The results of the kinematical refinements, presented in the supplementary documents, indicated a cation distribution similar to that reported in the literature, as well as in subsequent dynamical refinements, though with a relatively high R_{obs} (0.22, Table S1 in the ESI†). This high value suggests a significant discrepancy between the observed and calculated intensities, potentially due to unaccounted dynamical effects in the kinematical refinement. For a more accurate model based on electron diffraction data, it is essential to incorporate dynamical effects into the refinement process. A dynamical refinement was then carried out, aligning with the dynamical theory of diffraction, which accounts for the influence of both the structure factors and the crystal's orientation and thickness in the observed intensities. This adds complexity to the correlation between observed intensities and calculated structure factors, requiring the inclusion of multiple parameters during refinement to accurately account for these effects.[11]

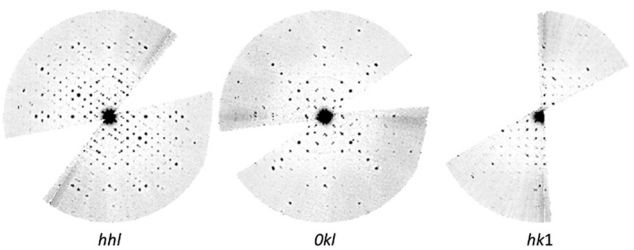

Fig. 2 Reconstructed reciprocal-space sections along three different directions confirming the reflection conditions of space group $Fd\bar{3}m$ (*hhl*: $h + l = 2n$; 0*kl*: $k + l = 4n$, and $k, l = 2n$; *hk*1: $h + k = 2n$ and $h + l, k + l = 2n$).

The initial kinematical refinement suggested a partial co-occupation of sites I and I′, but at the end of the refinement, the occupancies converged to 6.24 and 15.04 per unit cell (Table S2 in the ESI†), respectively. As a consequence, no crowding effect specific to "fully dehydrated" potassium-exchanged faujasite Y[7] and X,[12,13] is observed. The crowding is observable in several types of highly dehydrated faujasites with different Si/Al ratios. The extent of this crowding increases with the aluminum content (from K-Y to K-X)[7,12,13] reaching a maximum in the case of K-LSX,[14] where 16 K^+ ions occupy the SI site—slightly shifted from the centre of the hexagonal prism—and another 16 K^+ ions occupy the SI′ site.

Due to an incomplete dehydration inside the TEM sample chamber despite a high vaccum,[15] a restriction on the site occupation factors was introduced, with a starting distribution of 5.36 cations in site I and 18.11 in site I′ according to the structure of the dehydrated K-Y proposed by Mortier and Bosmans.[5,6] Subsequently, the cation distribution obtained from the dynamical refinement led to 7.70 K^+ in position I, 16.58 K^+ in position I′, 3.8 water molecules in position II′, and a full occupancy in site II with 32 K^+ (Table S3 in the ESI†). The different cation sites obtained from the dynamical refinement are shown in Fig. 3.

The water molecules at site II′ within the sodalite cages form a tetrahedral cluster. When they interact, water at site II′ and K^+ cations at site I′, they adopt a cubic arrangement (Fig. 3). These results align with the general trends found in the literature.[16,17] Furthermore, the kinematical and dynamical 3D ED refinement of the potassium exchanged nano-Y zeolite confirm the reliability of the methodology for determining the distribution of cations. Even with varying dehydration conditions and crystal sizes, the crystallographic sites I, I′, and II remain consistently occupied by K^+ cations in K-Y, with only slight variations in occupancy rates.

The bond distances and angles observed after the dynamical refinement of the K-Y nano FAU in 3D ED are reported in Table S4 of the ESI,† they are in line with those published,[5,7] further reinforcing the reliability of 3D ED for locating extra framework species in nano faujasites. The final R_{obs} was determined to be 0.11, and the refined composition was identified as $Si_{134.40}Al_{57.60}O_{389.03}K_{56.28}$. Further statistical indicators and details of the refinement parameters are shown in Table S1 of the ESI.†

To validate the 3D ED model, a Rietveld refinement was performed using high-resolution powder diffraction data collected at the ID22 beamline[18] of the European Synchrotron Radiation Facility (ESRF) on our sample dehydrated *in situ* (see experimental details in section 1.3 and 2.3 in the ESI†).

 This journal is © The Royal Society of Chemistry 2025

Published on 10 2025. Downloaded on 29/11/2025 00:12:04.

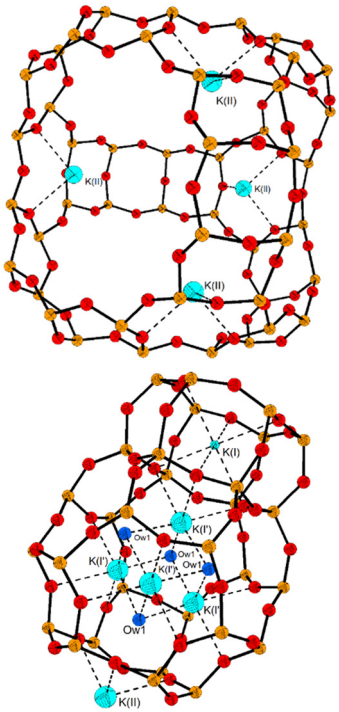

Fig. 3 Perspective view of the cation sites in nano-faujasite K-Y following dynamical refinement. Top: A supercage showing potassium cations occupying only site II. Bottom: A sodalite cage with an adjacent hexagonal prism, where cations are localized at sites I and I′. The refined occupancy factors are 0.481(1) for K(I), 0.518(1) for K(I′), 1 for K(II), and 0.1570(3) for Ow1. The number of water molecules is estimated as 75% of the refined occupancy factor of the Ow1 atom, assuming two hydrogen atoms per water molecule, giving approximately 3.8 H_2O per unit cell (0.157 × 32 × 0.75 ≈ 3.8 H_2O per u.c.).

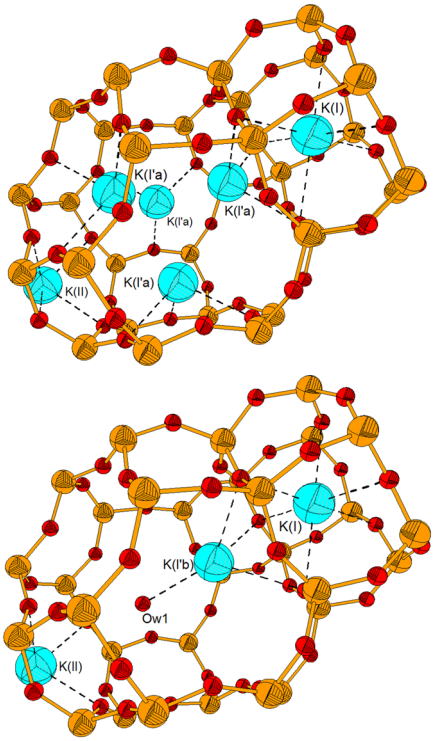

Fig. 4 Perspective view of the different cations environment in the sodalite cage of nano-faujasite K-Y following the Rietveld refinement at room temperature after dehydration *in situ* at 150 °C. Top: A sodalite cage with the non-hydrated site K(Ia′) represented. Bottom: The same with only site K(I′b) represented. The refined occupancy factors are 0.373(3) for K(I), 0.470(5) for K(I′a), 0.121(4) for K(I′b) and Ow1 and 1 for K(II). The number of water molecules is estimated as 75% of the refined occupancy factor of the Ow1 atom, assuming two hydrogen atoms per water molecule, giving approximately 2.9 H_2O per unit cell (0.121 × 32 × 0.75 ≈ 2.9 H_2O per u.c.). Selected bond lengths and angles are presented in Table S7 of the ESI.†

The validity of the 3D ED model is corroborated by the Rietveld refinement, which yields low *R*-factors and a satisfactory fit in the Rietveld plot (Table S5 and Fig. S6 in the ESI†). The refined composition of the nanozeolite after dehydration is $Si_{134.40}Al_{57.60}O_{387.87}K_{56.93}$ (Tables S5 and S6 in the ESI†), which closely matches the composition obtained in the TEM chamber. As in the 3D ED study, the supercage does not contain water molecules. However, in the powder sample, the cationic distribution within the sodalite cages shows slight variations (Table S6 in the ESI†). This can be attributed to the higher dehydration temperature used on beamline ID22, which resulted in greater water loss, as evidenced by Rietveld refinement showing 2.9 water molecules per unit cell. Site I′ is split into two distinct sub-sites, I′a and I′b, each associated with a different oxygen coordination environment, as illustrated in Fig. 4. Site I is slightly less occupied than in the 3D ED study, while site II remains fully occupied, consistent with the 3D ED findings.

In addition to the experimental approach, we have applied a Monte Carlo (MC) simulation technique, with a procedure successfully used for potassium X-type faujasite,[19] in order to describe the distribution of both potassium cations and water molecules along their crystallographic sites. The room temperature (298 K) canonical ensemble (NVT) MC simulations have been performed, with the 8.2.3 version of the Towhee code.[20,21] To conceive the microscopic model for the K-Y zeolite framework, the atomic positions for the T and oxygen atoms were taken from the IZA database and the unit cell parameter of the K-Y was set to the value of a = 24.85 Å, according to the literature data for a Y-type zeolite.[22] Then, 56 aluminum atoms were distributed along the T atoms, in accordance with the Loewenstein rule,[23] so that the unit cell chemical composition is given by the formula $K_{56}Si_{136}Al_{56}O_{384}$. The potassium cations distribution in the initial configuration, was set-up in a random manner. Interactions involving the zeolite atoms and water molecules were modeled using a sum of a 12-6 Lennard-Jones (LJ) term and a coulombic term electrostatic contribution. Lennard-Jones parameters and partial atomic charges describing zeolite atoms were taken from the Clay force field.[24] H_2O molecules were described by the TIP5P model.[21] The whole set of applied parameters is detailed elsewhere.[19] The potassium cations distribution in the initial configuration, was set-up in a random manner. The MC simulations were performed for several systems, varying by the number of water molecules per unit cell, comprised between 0 (totally

Published on 10 2025. Downloaded on 29/11/2025 00:12:04.

dehydrated zeolite) and 100. During the MC simulations, the framework atoms were maintained fixed, thus solely potassium cations and water molecules underwent displacements. In order to sample the configurational space, atom translation and intra-box swap MC moves were applied to potassium cations whereas water molecules were allowed to undergo centre-of-mass (COM) translation, COM rotation and intra-box swap. A MC run consisted 10^7 MC steps for the equilibration phase, followed by 2×10^7 MC steps for the production phase. During the production stage we recorded a configuration every 4000 MC steps. 2500 configurations generated in such manner were then analysed in order to describe the K^+ and H_2O distribution for each K-Y zeolite.

Table S8 in the ESI† summarizes the distributions of potassium cations for investigated water loadings, established through MC simulation. Inspecting how cationic distributions evolve with water content reveals a decrease of number of K^+ localized in small cages (*i.e.* hexagonal prism and sodalite cage, with cationic sites I, I′ and II′), passing from ~20 in dehydrated K-Y to ~14 in the 100 H_2O per u.c. containing K-Y. The number of cations in the large cage (*i.e.* supercage, with cationic sites II, III and III′) follows an opposite trend, increasing from 33.6 in dehydrated K-Y to 39.1, in the most hydrated one. This consistent evidence[25] is supported by cations coordinating water molecules, thus partially substituting the $K^+ \cdots O$ zeolite interactions, allowing cations to stabilize within the supercage, with increasing hydration. Moreover, the MC simulation results are illustrated in Fig. 5 and S7,† showing the snapshots cumulated through the 2500 configurations recorded across the production phase of the MC simulation runs.

Analysing the snapshots for the respective loadings of 5, 45 and 100 H_2O per u.c. (Fig. 5 and S7†) one can remark the presence of water molecules within both sodalite cages (approximately 20% of water loading), and supercages along all the reported hydration ratios. Within the sodalite cage, H_2O molecules are primarily localized at the crystallographic site designated as W1 by Hu *et al.*[26] which corresponds to Ow1 at site II′ in the present crystallographic study. This positioning allows water molecules to interact with cations located at sites I′.

Moreover, a minor fraction of the water molecules within the sodalite cages is located at crystallographic site I′. In the supercage, H_2O molecules are preferentially positioned near the 12-membered ring (12-MR) that separates adjacent supercages, where they interact with cations at site III′. These water molecules contribute to the formation of the so-called "ice-like structure", characterized by specific ring geometries within the 12-MR.[27] Regarding the simulated data, with the exception of K^+ cations at sites I, I′, and II, and water molecules within the sodalite cage at sites I′ or II′, all other cations at sites III and III′, as well as water molecules located in the supercage, exhibit extremely low occupancy factors when the symmetry of the space group $Fd\bar{3}m$ is considered. Although the dehydration level of our sample within the TEM is relatively high, it cannot be excluded—given the remaining dynamical effect together with the extremely low occupancy factors of some cations at sites III and III′, as well as residual water molecules at general positions—that these species cannot be reliably located using Fourier difference maps.

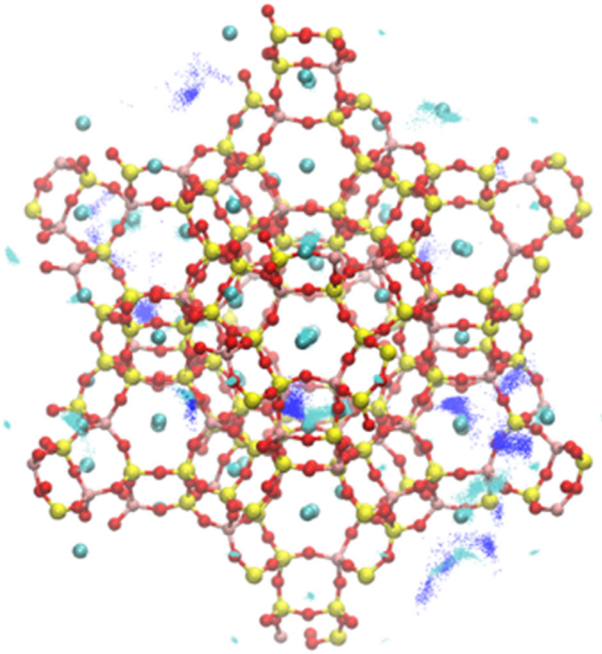

Fig. 5 Snapshots of the MC simulation results showing the loadings of 5 H_2O per u.c. in nano-faujasite K-Y. The yellow, orange, red, and cyan spheres represent silicon, aluminum, bridging oxygen atoms of the zeolite framework, and K^+ cations identified in the present 3D ED study, respectively. Blue dots indicate the oxygen atoms of water molecules, while cyan dots correspond to K^+ cations locations identified by simulations.

Conclusions

In conclusion, this study demonstrates the effectiveness of advanced electron diffraction techniques in investigating cation distributions in nano-zeolites. By employing 3D ED techniques, we overcame the limitations of conventional methods when applied to nanocrystals. Specifically, for nano-faujasite Y zeolite, this technique allowed us to elucidate the distribution of K^+ cations, which had previously been challenging due to the small crystal size and the effects of dynamical scattering. The use of precession electron diffraction (PED) in structural analysis, followed by kinematical and dynamical refinements using JANA2020, provided detailed insights into the distribution of K^+ cations across different crystallographic sites. In particular, the dynamical refinement significantly improved upon the kinematical results, yielding more accurate site occupancies, lower *R*-factors, refined atomic positions, and enabling localization of the majority of the remaining water molecules. These 3D ED results are further supported by a Rietveld refinement based on high-resolution synchrotron data collected after *in situ* dehydration at 150 °C, although the cation distribution within the sodalite cages differs slightly due to the increased dehydration rate at this temperature. The results are

 This journal is © The Royal Society of Chemistry 2025

Published on 10 2025. Downloaded on 29/11/2025 00:12:04.

consistent with trends observed in previous studies on faujasite-type zeolites with larger crystal sizes, even under different dehydration conditions. Crucially, however, this work represents the first comprehensive characterization of cation distribution from 3D ED in faujasite, a material that has been difficult to study with conventional methods. These findings underscore the importance of advanced techniques like 3D ED for investigating nanoscale zeolites. Moreover, these techniques lay the foundations for future research aimed optimizing the catalytic and/or adsorption properties of specific nano-zeolites by offering deeper insights into their local structure. However, the uncontrolled dehydration occurring within the TEM sample chamber at room temperature should be emphasized. To address this limitation, we plan—as a future direction of this work—to employ a cryogenic sample holder for crystallographic studies at higher hydration levels and varying temperatures. This approach may provide deeper insights into the cation migration process.

Data availability

Crystallographic data after the dynamical refinement and after the Rietveld refinement have been deposited at CCDC under deposition numbers CSD 2452355 and 2470815, they can be obtained from **https://www.ccdc.cam.ac.uk/structures/**. Other data supporting this article have been included as part of the ESI.†

Author contributions

Y. M. C. D.: investigation, writing – original draft. T. Ö. and I. D.: investigation, writing – review & editing. C. D.: investigation, writing. J.-L. P.: conceptualisation, investigation, writing – review & editing.

Conflicts of interest

There are no conflicts to declare.

Acknowledgements

The authors thank the University of Haute Alsace (UHA) for the Doctoral grant to Y. M. C. D. (Agreement No. 2022-58). I. D. would like to acknowledge the High Performance Computing Center of the University of Strasbourg for supporting this work by providing scientific support and access to computing resources. Part of the computing resources were funded by the Equipex Equip@Meso project (Programme Investissements d'Avenir) and the CPER Alsacalcul/Big Data.

References

1 J. V. Smith, in *Molecular Sieve Zeolites-I*, ed. E. M. Flanigen and L. B. Sand, American Chemical Society, 1974, ch. 15, vol. 101, pp. 171–200.
2 M. Gemmi and A. E. Lanza, *Acta Crystallogr., Sect. B: Struct. Sci., Cryst. Eng. Mater.*, 2019, **75**, 495–504.
3 M. Gemmi, E. Mugnaioli, T. E. Gorelik, U. Kolb, L. Palatinus, P. Boullay, S. Hovmöller and J. P. Abrahams, *ACS Cent. Sci.*, 2019, **5**, 1315–1329.
4 P. A. Midgley and A. S. Eggeman, *IUCrJ*, 2015, **2**, 126–136.
5 W. J. Mortier and H. J. Bosmans, *J. Phys. Chem.*, 1971, **75**, 3327–3334.
6 W. J. Mortier, H. J. Bosmans and J. B. Uytterhoeven, *J. Phys. Chem.*, 1972, **76**, 650–656.
7 W. T. Lim, S. Y. Choi, J. H. Choi, Y. H. Kim, N. H. Heo and K. Seff, *Microporous Mesoporous Mater.*, 2006, **92**, 234–242.
8 M. Borel, M. Dodin, T. J. Daou, N. Bats and J. Patarin, *New J. Chem.*, 2017, **41**, 13260–13267.
9 L. Palatinus, P. Brázda, M. Jelínek, J. Hrdá, G. Steciuk and M. Klementová, *Acta Crystallogr., Sect. B: Struct. Sci., Cryst. Eng. Mater.*, 2019, **75**, 512–522.
10 V. Petříček, M. Dušek and L. Palatinus, *Z. Kristallogr. - Cryst. Mater.*, 2014, **229**, 345–352.
11 L. Palatinus, C. A. Corrêa, G. Steciuk, D. Jacob, P. Roussel, P. Boullay, M. Klementová, M. Gemmi, J. Kopeček, M. C. Domeneghetti, F. Cámara and V. Petříček, *Acta Crystallogr., Sect. B: Struct. Sci., Cryst. Eng. Mater.*, 2015, **71**, 740–751.
12 L. Zhu and K. Seff, *J. Phys. Chem. B*, 2000, **104**, 8946–8951.
13 L. Zhu and K. Seff, *J. Phys. Chem. B*, 2001, **105**, 12221–12222.
14 H. Guesmi, P. Massiani, H. Nouali and J.-L. Paillaud, *Microporous Mesoporous Mater.*, 2012, **159**, 87–95.
15 T. Örs, I. Deroche, C. Chatelard, M. Dodin, R. Martinez-Franco, A. Tuel and J.-L. Paillaud, *Symmetry*, 2024, **16**, 477.
16 G. R. Eulenberger, D. P. Shoemaker and J. G. Keil, *J. Phys. Chem.*, 1967, **71**, 1812–1819.
17 J. J. I. Van Dun, W. J. Mortier and J. B. Uytterhoeven, *Zeolites*, 1985, **5**, 257–260.
18 A. Fitch, C. Dejoie, E. Covacci, G. Confalonieri, O. Grendal, L. Claustre, P. Guillou, J. Kieffer, W. de Nolf, S. Petitdemange, M. Ruat and Y. Watier, *J. Synchrotron Radiat.*, 2023, **30**, 1003–1012.
19 T. Ammouli, J.-L. Paillaud, H. Nouali, R. Stephan, M.-C. Hanf, P. Sonnet and I. Deroche, *J. Phys. Chem. C*, 2021, **125**, 19405–19416.
20 M. G. Martin, *Mol. Simul.*, 2013, **39**, 1212–1222.
21 M. W. Mahoney and W. L. Jorgensen, *J. Chem. Phys.*, 2000, **112**, 8910–8922.
22 J. M. Kneller, T. Pietraß, K. C. Ott and A. Labouriau, *Microporous Mesoporous Mater.*, 2003, **62**, 121–131.
23 W. Loewenstein, *Am. Mineral.*, 1954, **39**, 92–96.
24 R. T. Cygan, J.-J. Liang and A. G. Kalinichev, *J. Phys. Chem. B*, 2004, **108**, 1255–1266.
25 W. Louisfrema, B. Rotenberg, F. Porcher, J.-L. Paillaud, P. Massiani and A. Boutin, *Mol. Simul.*, 2015, **41**, 1371–1378.
26 M. Hu, J. C. Hanson and X. Wang, *Ind. Eng. Chem. Res.*, 2018, **57**, 4988–4995.
27 C. A. C. Perez, N. S. de Resende, V. M. M. Salim and M. Schmal, *J. Phys. Chem. C*, 2017, **121**, 2755–2761.